

4-11-1-58

A Study of Inclusions Causing Fatigue Cracks in Steels for Carburized and Shot-Peened Gears*

Takeshi TOYODA**
Takashi KANAZAWA**
Kazuaki MATSUMOTO**

The fatigue fractures of carburized and shot-peened gears tend to be caused by the non-metallic inclusions under the surface because the fatigue strength of the surface of the gears is improved by shot peening operations. This paper discusses the quantitative relationship between the size and locations of the inclusions, and the fatigue strength. The fatigue strength values were obtained by rotating bending fatigue tests of a newly developed clean steel for carburized gears. Also discussed is the clean steel's remarkably improved fatigue strength.

1. Introduction

There has been an increasing need for stronger and more reliable power-train parts such as gears and shafts because motor vehicles are getting lighter and engines are becoming more powerful. Carburized steel is used for gears and recently carburized gears strengthened by shot peening have come into wide use.

With shot peening, crack initiation of fractures tends to shift from the surface toward the subsurface of carburized gears because the fatigue strength of shot peened gears' surface is improved by the development of compressive residual stress and hardness in the surface layers.^{(1),(2)}

It is well known that the crack initiation of subsurface initiated fractures often occurs at a non-metallic inclusion existing in the steel. The objective of this report is to investigate the effects of the non-metallic inclusion on the fatigue strength of carburized and shot-peened steel. Rotating bending fatigue tests were carried out using steels with different oxygen content. The size and the location of inclusions apparent on the fracture surface was observed.

2. Specimens and experimental procedure

The chemical composition of Cr-Mo steel (JIS SCM420H) used in this study is shown in Table 1. A steel had conventional oxygen content of 21ppm and the oxygen content of B steel was reduced to 9ppm. $\phi 25$ specimens and $\phi 6$ specimens shown in Fig. 1 were machined from normalized steel bars. The specimens were gas carburized to the total case depth of 1.0mm.

Steel	C	Si	Mn	P	S	Cr	Mo	t.O
A	0.22	0.27	0.79	0.018	0.007	1.11	0.18	0.0021
B	0.19	0.28	0.79	0.007	0.018	1.12	0.17	0.0009

Table 1 Chemical composition (ladle analysis, %)

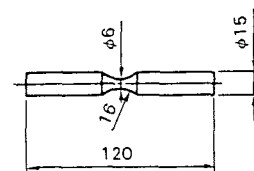
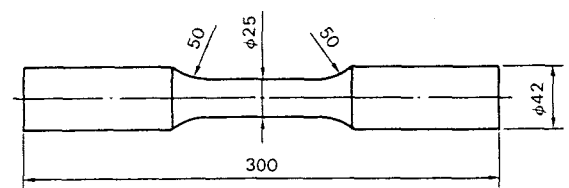


Fig.1 Shape of specimens

* Received 4th October, 1989
** Research Engineer
Material Development Dept.
Isuzu Motor Limited
25-1, Tonomachi 3-chome, Kawasaki-ku, Kawasaki-shi,
Kanagawa-ken, 210 Japan
*** Research Engineer
Steel Research Center
NKK Corporation
1-1, Minamiwatarida-cho, Kawasaki-ku, Kawasaki-shi,
Kanagawa-ken, 210 Japan

Two shot peening treatments are summarized in Table 2. X treatment was done by the conventional centrifugal wheel-type shot peening with arc height of 0.45A. Y treatment was done by the new air nozzle type shot peening with arc height of 0.30C (e.q. 1.10A). Rotating bending fatigue tests were performed using both X-peened and non-peened $\phi 25$ specimens, and X and Y-peened and non-peened $\phi 6$ specimens.

Type	Size	Hardness	Coverage	Arc height
X Centrifugal wheel	$\phi 0.8\text{mm}$	HRC 53	300%	0.45A
Y Air nozzle				0.30C (e.q. 1.1A)

Table 2 Shot peening treatment

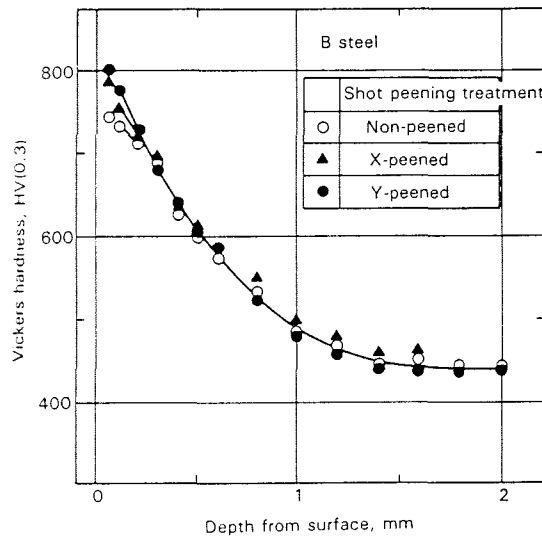


Fig.2 Influence of shot peening on microhardness distribution

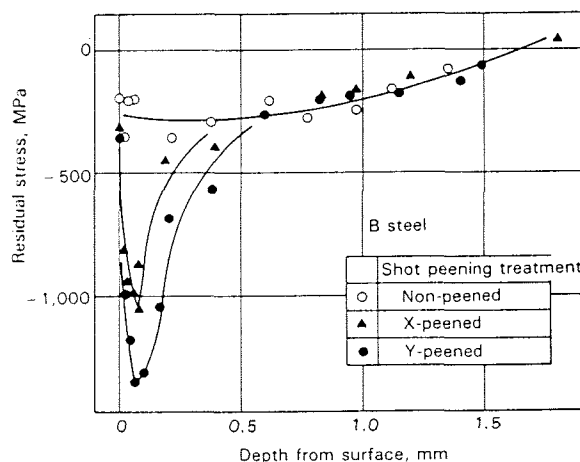


Fig.3 Influence of shot peening on residual stress distribution

Figure 2 shows the hardness distributions in the surface layers of B steel $\phi 6$ specimens. The Vickers hardness of the subsurface becomes higher with shot peening. The hardness distributions of the different steels were nearly identical.

The residual stress distributions of B steel $\phi 6$ specimens are shown in Fig.3. By shot peening, higher compressive stresses, for example $-1,100\text{MPa}$ in X-peened specimens and $-1,400\text{MPa}$ in Y-peened specimens, are induced near the surface. The residual stress distributions of the different steels were similar.

3. Experimental results and discussion

3.1. Results of the rotating bending fatigue tests

The results of the fatigue tests of $\phi 25$ specimens are shown in Fig.4. For lives shorter than 3×10^5 cycles, the crack initiation was found to be surface-initiated. At lives higher than this, the fatigue crack originated in the sub-surface, and a fish eye was observed on the fracture surface. As the slope of the applied stress distribution was gradual in the case of the $\phi 25$ specimen, the crack initiations at higher lives were found to be in the subsurface in non-peened specimens too. Therefore, shot peening cannot increase the fatigue strength of $\phi 25$ specimens. However, in a comparison of A steel and B steel, B steel with lower oxygen content has fatigue strength about 9% higher than that of A steel.

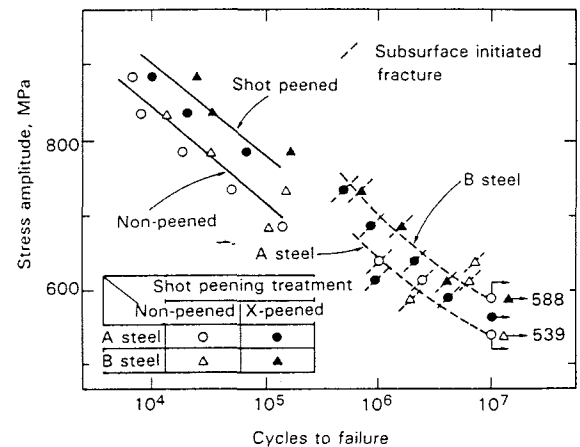


Fig.4 S-N curves of $\phi 25$ specimens

The results for $\phi 6$ specimens are shown in Fig.5 and Fig.6. In the case of $\phi 6$ specimens, the fatigue strength is increased by shot peening because the fatigue crack starts at the surface in non-peened specimens by the reason of the sharp slope of the applied stress distribution. Y-peening cannot increase the fatigue strength of A steel more than X-peening because the crack initiation site is shifted from the surface toward the sub-

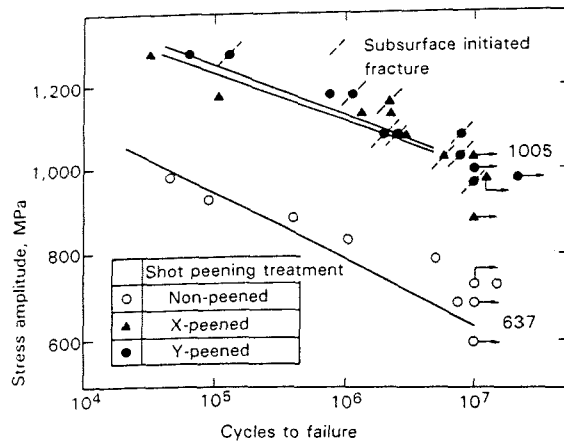


Fig. 5 S-N curves of $\phi 6$ specimens (A steel)

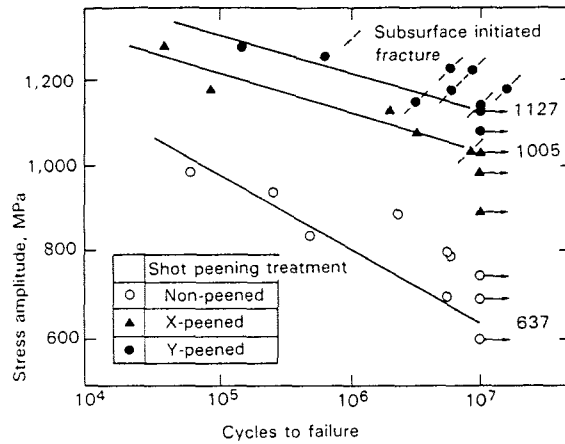


Fig. 6 S-N curves of $\phi 6$ specimens (B steel)

surface by X-peening. On the other hand, in the case of B steel with lower oxygen content, the fatigue strength of Y-peened specimens was increased by about 12% more than that of X-peened specimens because the crack originated at the surface in spite of X-peening.

In summary, it is necessary, in order to increase the fatigue strength by shot peening, that the surface layers be strengthened by more powerful shot peening to

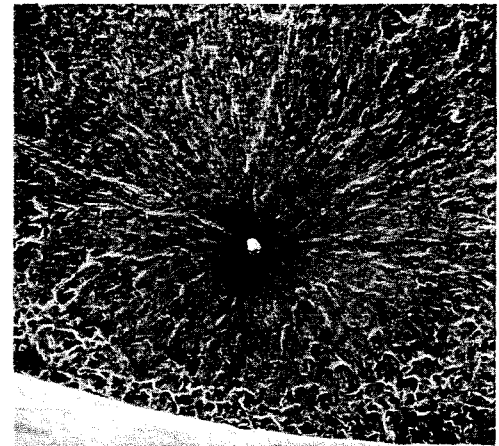


Fig. 7 SEM fractograph with crack initiation at subsurface non-metallic inclusion

develop larger compressive residual stresses, and that the fatigue strength of the subsurface be improved by decreasing the oxygen content to reduce the non-metallic inclusions.

3.2. Results of fractography

An example of an SEM fractograph with crack initiation at a subsurface non-metallic inclusion is shown in Fig. 7. The fatigue crack originated at the center of the smooth, flat circle in the fracture surface. The fatigue crack was propagated at slow speed from the initiation site, and the fracture advanced rapidly after the fatigue crack reached the surface. Non-metallic inclusions induced fractures in the most case of subsurface-initiated fractures. The inclusions were an $Al-Ca-O-S$ complex according to the results of analysis by an electron probe micro analyzer.

The size (diameter), the depth from the surface, and the axial offset from the center of the inclusions causing the fracture are shown in Table 3. The average size of the inclusions of B steel is smaller than that of inclusions of A steel. The size of the inclusions of $\phi 6$ specimens is smaller than of $\phi 25$ specimens.

The location of the inclusions of A steel is little different from that of the inclusions of B steel, but one of the $\phi 25$ specimens is very different from the $\phi 6$ speci-

		$\phi 25$		$\phi 6$	
		A steel	B steel	A steel	B steel
Location	Depth from surface (mm)	1.4 – 2.6 $\bar{X}=2.0$	1.3 – 2.4 $\bar{X}=2.0$	0.25 – 0.76 $\bar{X}=0.40$	0.24 – 0.76 $\bar{X}=0.45$
	Axial offset from center (mm)	1.5 – 26.6 $\bar{X}=13.5$	11.2 – 24.6 $\bar{X}=16.8$	0.1 – 1.5 $\bar{X}=0.50$	0.2 – 2.0 $\bar{X}=1.09$
Diameter of inclusions (μm)		33.8 – 71.0 $\bar{X}=47.3$	13.9 – 53.4 $\bar{X}=30.0$	10.0 – 48.2 $\bar{X}=26.9$	9.6 – 27.0 $\bar{X}=16.7$

Table 3 Size and location of the inclusions causing fatigue cracks

mens. Inclusion-originated fatigue cracks in $\phi 25$ specimens were observed near the case-core interface or inside the core (1.3 – 2.6mm depth from the surface), whilst they were observed in the carburized case (0.2 – 0.8mm depth from the surface) in $\phi 6$ specimens.

3.3. Relationship between the size of the inclusions and the fatigue strength

Murakami et al.^[3] estimated the results of fatigue tests using the parameter of the projected area of the principal stress direction of the defect, when discussing the influence of inclusions and small defects on fatigue strength.

We tried to estimate the influence of inclusions on the fatigue strength by the following experimental equation based on Murakami's equation with due regard for the residual stress induced by carburizing and shot peening.

$$\sigma_w = 1.56(HV + 120)/(\sqrt{area})^{1/6} - \sigma_r/2 \quad (1)$$

σ_w : fatigue strength (MPa)

HV : Vickers hardness in crack initiation site

area : projected area of the principal stress direction of the inclusions (μm^2)

σ_r : residual stress (MPa)

Figure 8 shows the relationship between the ratio of nominal applied stress σ' at the crack initiation site to fatigue strength σ_w estimated according to equation (1) and the number of cycles to failure Nf (with $\phi 25$ specimen).

The linear relationship between σ'/σ_w and Nf is expressed and is similar to S-N curves for both $\phi 25$ and $\phi 6$ specimens. As the σ'/σ_w value is 1.0 at 10^7 cycles, it is found that the fatigue strength can be estimated from the size of the inclusions, the hardness and the residual stress at the crack initiation site.

Figure 9 shows the critical size of inclusions estimat-

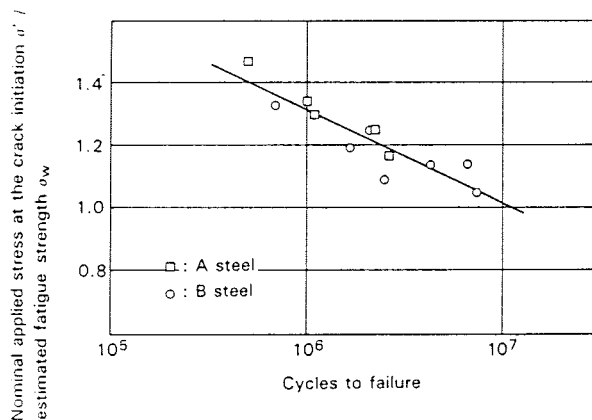


Fig.8 Relationship between the ratio of the nominal applied stress σ' at the crack initiation site to estimated fatigue strength σ_w and number of cycles to failure ($\phi 25$ specimens)

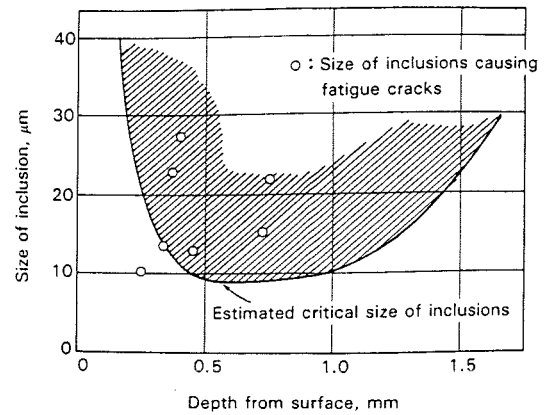


Fig.9 Relationship between estimated critical size of inclusion and size of inclusions causing fatigue cracks ($\phi 6$ specimens, B steel, fatigue strength: 1127MPa)

ed according to equation (1), by measuring HV and σ_r (ex. $\phi 6$ specimen). The critical size of the inclusions is large in the sub-surface and drops markedly at 1.1mm under the surface for $\phi 25$ specimens and to 0.2mm for $\phi 6$ specimens, and then increases gradually. The size of inclusions causing fatigue fracture exceeds the critical size, and the location of crack initiation site nearly conforms to the calculation results.

3.4. Relationship between the number of inclusions in steel and the fatigue strength

A number of large inclusions over $20\mu m$ in diameter in steel are shown in Fig.10. In the measurement process, 5g of steel were dissolved in 500ml of (1+3)HNO₃ and then the residue was extracted by a fine-mesh metal filter of $20\mu m$ mesh size for the purpose of counting the number of inclusions under a microscope.

The number of inclusions over $20\mu m$ is decreased remarkably by the reduction of oxygen content in steel. It is found that the decrease of the number of large in-

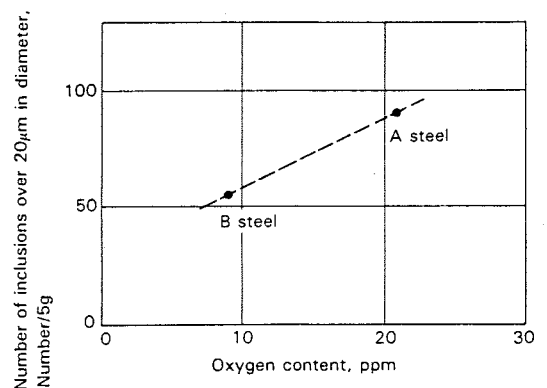


Fig.10 Relationship between oxygen content and number of inclusions

clusions strengthens low-oxygen steel, as the mean size of the inclusions observed on subsurface-initiated fractures for B steel is smaller than for A steel.

The number of inclusions over 20 μm existing in the domain that may be the crack initiation site (danger zone) is shown in Table 4. It is found that about 2 — 4 inclusions of size equivalent to that of inclusions causing subsurface initiated fractures exist in the danger zone.

	Fatigue strength (MPa)	Average size of inclusions causing fatigue cracks	Volume of danger zone (V)	Number of inclusions over 20 μm existing in Vg of steel
A steel	1005	25 μm	0.23g	4.1
B steel	1127	17 μm		2.5

Table 4 Number of inclusions over 20 μm existing in danger zone

4. Summary

- (1) The low-oxygen steel in which non-metallic inclusions are decreased exhibits higher fatigue 9 — 12% strength than that of conventional steel in the case where the crack initiation originates under the surface of both $\phi 25$ specimens (the crack originates at the case-core interface) and $\phi 6$ specimens (the crack originates in the carburized case).
- (2) The influence of the inclusions on the fatigue strength is estimated by the following equation, which adds the residual stress to Murakami's equation.

$$\sigma_w = 1.56(\text{HV} + 120)/(\sqrt{\text{area}})^{1/6} - \sigma_r/2$$

σ_w : fatigue strength (MPa)

HV : Vickers hardness at crack initiation site

area : projected area of the principal stress direction of the inclusions (μm^2)

σ_r : residual stress (MPa)

- (3) As the above results show, it is found out that not only addition of high compressive residual stress by high-strength shot peening but also decreasing the non-metallic inclusions by reducing the oxygen content are necessary in order to strengthen carburized steel.

References

- (1) Hisamatsu, S. and Kanazawa, T., JSMS, 29th Symposium (in Japanese), (April 1980)
- (2) Kanazawa, et al., JSAE Symposium (in Japanese), (May 1988)
- (3) Murakami, Y. and Shimizu, M., Trans. Japan Soc. Mech. Engrs. (in Japanese), Vol.54, No.499 (Mar. 1988), P.413